

DYNAMIC BEHAVIOUR OF GREEK POST-BYZANTINE CHURCHES WITH FOUNDATION DEFORMABILITY AND EVALUATION OF THEIR EARTHQUAKE PERFORMANCE – EXPERIMENTAL INVESTIGATION OF STONE MASONRY MATERIAL PROPERTIES

G.C. Manos¹, L. Kotoulas^{1*}, V. Matsou¹, O. Felekidou¹

¹Laboratory of Strength of Materials and Structures
Dept. Civil Engineering, Aristotle University of Thessaloniki
University Campus, Egnatia street, Thessaloniki, 54006
gcmanos@civil.auth.gr

Keywords: Post-Byzantine Churches, Numerical Simulation, Deformable Foundation, Experimental study of stone masonry, Retrofitting.

Abstract. *The earthquake performance of stone masonry Post-Byzantine churches subjected to seismic forces is examined. The examined churches are: 1. A three-nave Basilica with a system of stone-masonry vaults and domes as a superstructure together with a wooden roof. 2. An 18th century church of the cruciform type which also utilizes a system of cylindrical vaults and spherical domes that form the superstructure together with the wooden roof. 3. A three-nave 18th century Basilica whose the wooden roof is supported directly on the peripheral masonry walls and the internal colonnades. All these churches developed structural damage to the masonry elements that is believed to arise from the amplitude of the gravitational and seismic actions combined with the deformability of the foundation, a parameter that is also part of this investigation. The numerical results together with assumed strength values are utilized to predict the behaviour of the various masonry parts in in-plane shear and normal stress as well as out-of-plane flexure. It is demonstrated that the foundation deformability explains, partly, the appearance of structural damage. When comparing the numerically predicted regions that reach limit state conditions with actual damage patterns a reasonably good agreement in a qualitative sense can be observed. The masonry walls near the foundation, the door and window openings, and the roof appear to be the most vulnerable either in out-of-plane bending or in in-plane shear for the critical combination of seismic forces and gravitational loads. Moreover, the vaults and domes of the superstructure appear to be vulnerable also. A relatively mild retrofitting scheme that utilizes special mortar injections as well as semi-temporary shoring together with wooden and metal ties is then examined. This is also investigated numerically being applied to a 16th Century Basilica with a wooden roof. The numerical investigation is supplemented with a series of limited Laboratory tests on the constituent materials represented by old stone masonry.*

1 INTRODUCTION

During the last thirty years various parts of Greece have been subjected to a number of damaging earthquakes ranging from $M_s=5.2$ to $M_s=7.2$ on the Richter scale. One of the most demanding tasks for counteracting the consequences of all these seismic events was the effort to ensure the structural integrity of old churches, that were built in periods ranging from 400 A.D. up to today; in many cases they sustained considerable damage [1]. The earthquake behavior of churches belonging to the so-called Post-Byzantine period (16th to 19th century A.D.) has been studied numerically in some detail ([2], [3], [4], [5], [6], [7], [8]). In all these cases the foundation was considered to be non-deformable. However, this is a gross approximation as in most cases these churches are founded on deformable soil. In some instances, the deformability of the soil caused considerable damage as is the case of the church of The Assumption of the Virgin Mary at Dilofo-Voio-Kozani, as will be presented in section 2. In some other cases the main cause of recent damage is the earthquake activity that is accentuated by the deformability of the soil. This will be presented in the sections 3 and 4, where the damage of the church of Agia Triada at Vithos-Kozani and of Profitis Elias at Siatista-Kozani is also included. Finally, in section 5 as a summary of retrofitting principles together with brief results from a relevant numerical and experimental investigation focusing on the behavior of St. Dimitrios of Palatitsia is also presented. It must be noted that these churches were built in a number of phases on old existing sacred sites by extending old remains, due to prohibitions by the Turkish occupation authorities imposed on the Christian population forbidding the construction of new churches but only allowing the maintenance of existing ones, after special permit [19].

2 THE ASSUMPTION OF THE VIRGIN MARY AT DILOFO-VOIO-KOZANI

The outlay of this church is shown in figure 1 by a cross-section in the longitudinal direction. Its basic dimensions are 21.5m long (together with the apse of the East wall) 11m wide and a maximum height to the top of the wooden roof 10m. With the dashed line the hard-soil is indicated. As can be seen, the West part of this church is founded on hard soil (weathered flysch layers) whereas the East part is founded on relatively soft soil that was deposited on top of the layers to compensate for the natural slope at this location. Apart from the relatively soft soil deposits at the East part of this church the malfunction of the drainage system at this point initiated considerable settlement of these soft soil deposits.

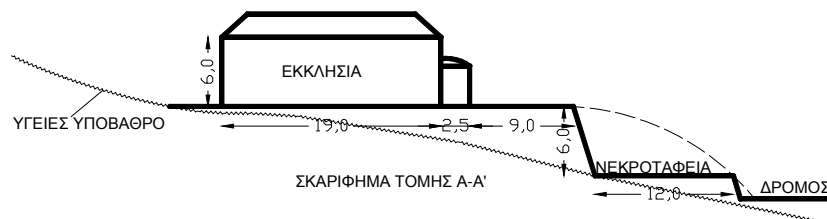


Figure 1. The layout of the church of the Assumption of Virgin Mary

The unequal settlement of the foundation of the stone masonry walls as well as of the internal columns that supported the vaulting system, which covered this church, caused considerable damage. An external view of this church from the South is shown in figure 2a whereas figure 2b depicts the extensive damage that developed at the South-East corner. A very wide crack initiates at the top of the East peripheral wall near the apse and propagates towards the bottom of this wall being inclined to the South-East corner. Furthermore, a similarly wide crack propagates through the North peripheral wall from top to bottom as is shown in figure 2c. It must be noted that the thickness of these masonry walls varies from 750mm to 800mm.

From this extensive peripheral wall damage, the vaulting system that is supported by these peripheral walls also suffered extensive cracking that eventually caused the partial collapse of a part of the central dome, as shown in figure 2d.



Figure 2a. Side view from the South



Figure 2b. Damage to the South-East corner



Figure 2c. Damage to the North wall



Figure 2d. Partial collapse of the central dome

2.1. Numerical Simulations

Initially, the numerical simulation assumed that the foundation was non-deformable [9]. Based on this assumption the 3-D numerical representation of the church, including the peripheral walls, the vaulting system of the superstructure, as shown, and the wooden roof were subjected to load combinations of either $0.9G \pm 1.4E_x$ or $0.9G \pm 1.4E_y$, where G is the gravitational load and E_x , E_y the earthquake forces ([10]) along the x-x axis (longitudinal East-West direction) or the y-y axis (transverse North-South direction, respectively).

Non - Deformable Foundation

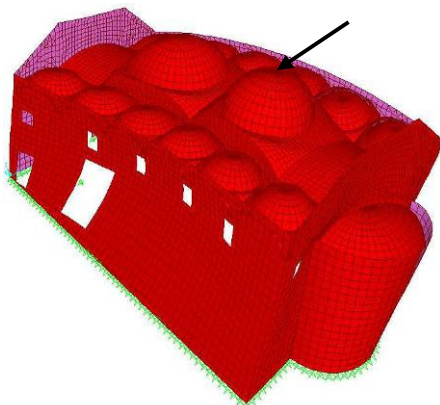


Figure 3a. Displacement Response. $0.9G+1.4(+E_x)$
 $U_x = 6.81 \text{ mm}$ $U_z = -1.51 \text{ mm}$

. Deformable Foundation

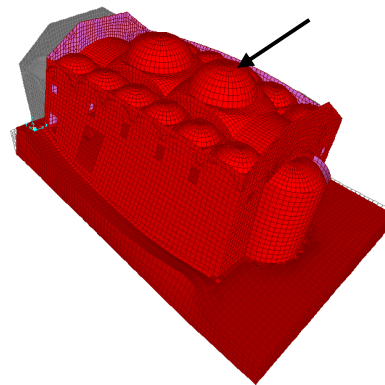


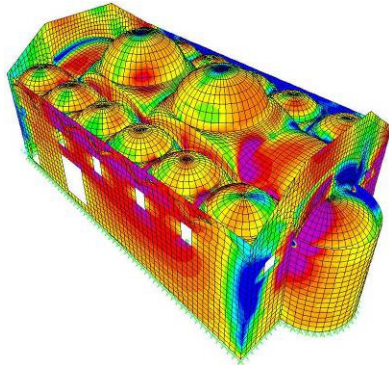
Figure 3b. Displacement Response. $0.9G+1.4(+E_x)$ $U_x = 21.33 \text{ mm}$ $U_z = -14.80 \text{ mm}$

All the supports were assumed to prohibit the translations along all three axes but not to restrain the rotations. It was found from previous studies that full fixity of the masonry walls at the foundation level leads to the development of considerable bending moments that corre-

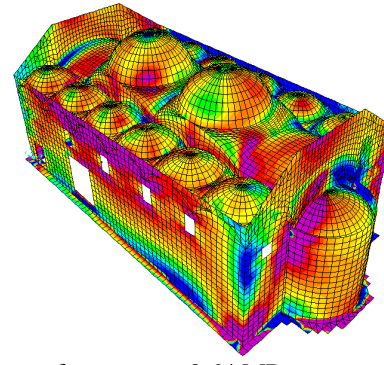
spond to tensile stresses which cannot be sustained by the weak stone masonry used to construct these churches. For the load combination $0.9G+1.4(+Ex)$ the maximum deformations at the top of the central dome were found equal to $U_x = 6.81$ mm $U_z = -1.51$ mm (figure 3a). For this load combination the maximum tensile stresses parallel to the bed joint σ_{11} were found equal to 0.51 MPa, at the bottom face of the masonry walls (figure 4a). As can be seen in this figure, high tensile stresses parallel to the bed joint develop both at the top of the North wall as well at the South-East corner of the East wall.

Non - Deformable Foundation

Deformable Foundation



a) σ_{11} bottom face, $\max\sigma = 0.51$ MPa.



b) σ_{11} bottom face $\max\sigma = 0.64$ MPa

Figure 4. Out-of-plane behavior, Load Combination $0.9G+1.4(+Ex)$

2.1.1. Numerical Simulation of the state of stress arising from the foundation settlement.

Next, layers of deformable soil were introduced beneath the foundation of all the peripheral walls and internal colonnades. The stiffness of these soil layers was varied in order to simulate the relatively hard soil at the West part of the church and the relatively soft soil at the North-East part of the church (see figure 1). For quantifying the stiffness of these soil layers use was made of the data from three boreholes drilled at the vicinity of the church relevant to the constitution of the soil deposits at a depth up to 10m [9]. For the load combination $0.9G+1.4(+Ex)$ the maximum deformations at the top of the central dome were found equal to $U_x = 21.33$ mm $U_z = -14.80$ mm (figure 3b); these values represent a considerable increase in the deformation at the top of the church from the previous case where the soil was considered non-deformable. Figure 4b depicts the distribution of stresses σ_{11} parallel to the bed joint; the maximum tensile values were found equal to 0.64 MPa, at the bottom face of the masonry walls. As can also be seen in this figure, high tensile stresses parallel to the bed joint develop both at the top of the North wall and at the South-East corner of the East wall. The increase in the tensile stresses for the deformable soil is of the order of 30% to 50% when compared to the corresponding maximum tensile stresses when the soil was considered non-deformable. As could be seen from the preceding numerical study, the uneven deformability of the soil under the foundation of such structural formations, as Post-Byzantine Basilica churches, can introduce an increase in the critical tensile stresses. The regions of the masonry elements where such tensile stress concentration appear correlate reasonably well with the areas of damage that was observed in this church.

3 THE AGIA TRIADA (HOLY TRINITY) AT VITHOS-VOIO-KOZANI

This is a Post-Byzantine church of the cruciform type with three domes. There is a central dome that rises at the highest elevation to 15.75m from ground level, whereas the length of

the church in the longitudinal East-West direction is 17.60m and its width in the North-South direction is 9.85m. The construction of this stone-masonry church was completed in 1797 A.D. using the local natural stone. The plan and the East-West cross-section are shown in figures 5a and 5b.

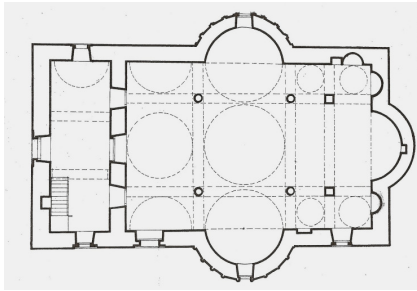


Figure 5a. Plan



Figure 5b. East-West section, View from the South



Figure 5c. View from the South-West



Figure 5d. View from the North

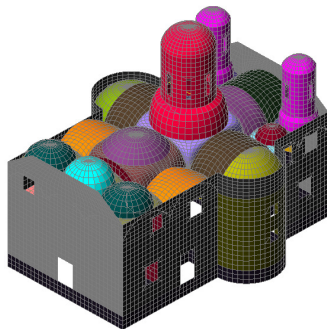


Figure 5e. View from the South-West

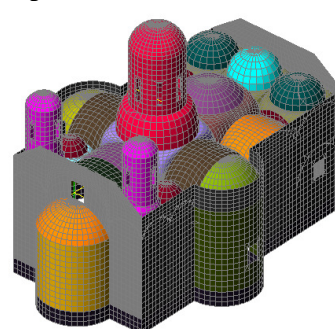


Figure 5f. View from the North-East

The vaulting system that supports the three domes is depicted in figures 5a to 5f, as can be seen from the top by removing the wooden roof. The numerical simulation considered two distinct models. The first model assumed non-deformable foundation where the translations along the three axes (x , y , z) were restrained to zero.

The second model tries to account for the deformability of the foundation by using as supports linear springs with stiffness properties that were estimated taking into consideration the quality of the underlying media (figure 6) as well as the thickness of the foundation and the discretization employed.

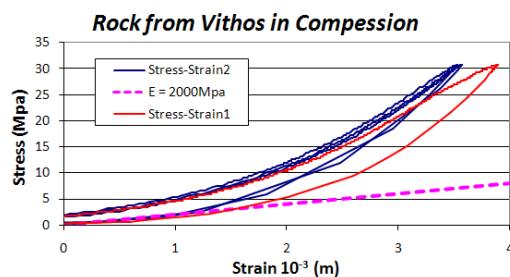
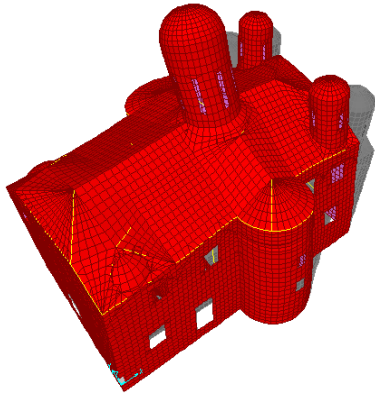
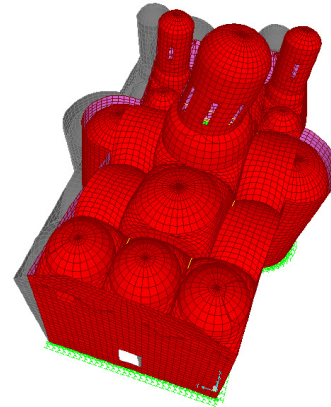


Figure 6. Compressive stress-strain behaviour of a slate sample taken from the vicinity of the church



Non-deformable foundation

Figure 7a. 1st Translational eigen-mode y-y, $T_y = 0.154$ sec modal mass ratio $U_y = 44.67\%$



Deformable foundation

Figure 7b. 1st Translational eigen-mode y-y, $T_y = 0.197$ sec modal mass ratio $U_y = 60.26\%$

The modal analysis results, depicted in figures 7a and 7b, demonstrate the first effect of the deformable foundation which is the lengthening of the eigen-periods of the most significant translational modes as well as the mobilization of larger modal mass ratios for these eigen-modes when the deformable foundation was considered as compared to the corresponding values of the non-deformable foundation.

Next, the deformations of the structural system were obtained for both the non-deformable and the deformable foundation model. These were obtained for two sets of load combination. The first is designated as $0.9G + 1.4E_x$ and signifies the combination of the gravitational forces (G) with the seismic actions in the East-West (x-x) longitudinal direction. The seismic action was enforced by applying the dynamic spectral method with a design spectrum specified by the current Greek Seismic Code and for seismic Zone I and soil category A [10]. The second load combination is designated as $0.9G + 1.4E_y$ and signifies the combination of the gravitational forces (G) with the seismic actions in the North-South (y-y) transverse direction. The results are depicted in figures 8a to 8d.

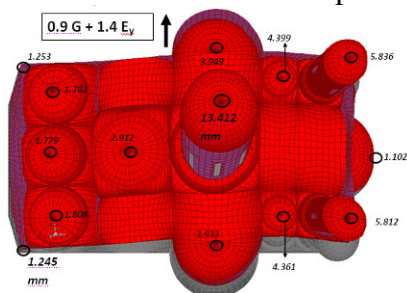


Figure 8a. $0.9G + 1.4E_y$, Non-Deformable Foundation Max. Disp. Top central dome 13.442mm

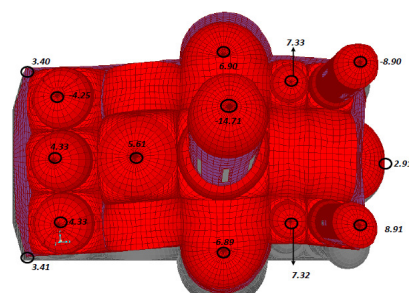


Figure 8b. $0.9G + 1.4E_y$, Deformable Foundation Max. Disp. Top central dome 14.640mm

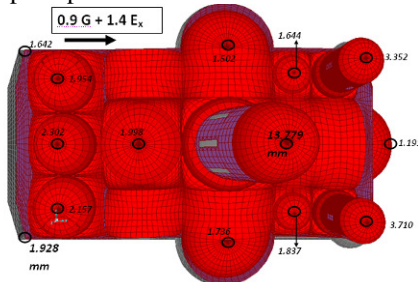


Figure 8c. $0.9G + 1.4E_x$ Non-Deformable Foundation Max. Disp. Top central dome 13.779mm

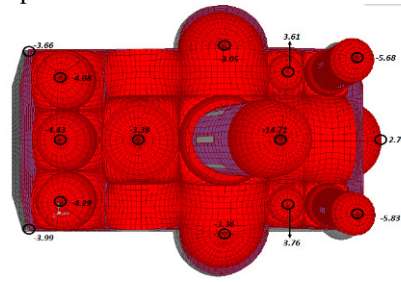


Figure 8d. $0.9G + 1.4E_x$ Deformable Foundation Max. Disp. Top central dome 14.710mm

Due to the foundation deformability the earthquake actions combined with the gravitational forces result in a considerable increase in the horizontal displacement response. This is more pronounced at the top of the peripheral wall where the vaults of the superstructure and roof are supported than at the top of the central dome level. At that level, the maximum displacement is equal to 14.710mm for the deformable foundation and 13.779mm for the non-deformable foundation for the load combination $0.9G+1.4E_x$. For the load combination $0.9G+1.4E_y$ the maximum displacement at the top of the central dome level is 13.442mm for the non-deformable foundation as compared with 14.640mm for the deformable foundation. Similar influence of the foundation deformability can also be observed in the maximum stress values that develop at either the peripheral walls, the internal transverse wall or at parts of the vaulting system of the superstructure.

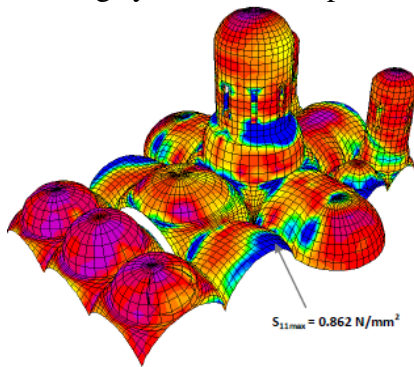


Figure 9a. $0.9G+1.4E_x$ Non-Deformable Foundation top face Max. Tensile σ_{11} 0.862Mpa

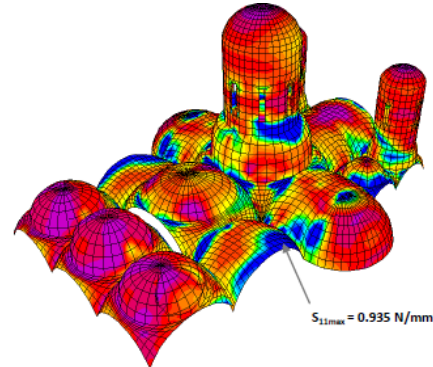


Figure 9b. $0.9G+1.4E_x$ Deformable Foundation top face Max. Tensile σ_{11} 0.935Mpa

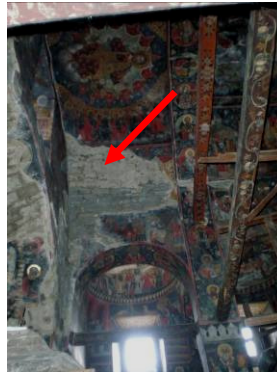


Figure 9c. Damage of the vaulting system

Figures 9a and 9b depict the tensile stress concentration at the outer (top) face of the vaulting system, as it results from either load combination $0.9G+1.4E_x$ or $0.9G+1.4E_y$. As can be seen, the foundation deformability increases the tensile stress demand at critical locations for the vaulting of the superstructure. This observation, which is based on the numerical results, is also supported by in-situ evidence of damage to the masonry parts of the vaulting system, as shown in figures 9c.

Table 1 lists the assumed mechanical characteristics for the stone masonry in terms of Young's modulus and Poisson's ratio as well as compressive and tensile strength values [11]. Moreover, a Mohr-Coulomb failure envelope was adopted for the in-plane shear limit state of the stone masonry, when a σ_n stress is acting normal to the mortar bed joint simultaneously with the shear, that is defined through relationship (1) ([2], [3], [4], [5], [6], [7], [8], [11]).

$$f_{vk} = f_{vko} + 0.4 \sigma_n \quad (1)$$

where: f_{vko} is the shear strength of the stone masonry when the normal stress σ_n is zero; f_{vko} was assumed to be equal to 0.192 N/mm², a relatively high value.

	Young's Modulus (N/mm ²)	Poisson's Ratio	Compressive Strength (N/mm ²)	Tensile Strength normal / parallel bed-joint (N/mm ²)	shear strength f_{vko} (N/mm ²)
Limit values	2500	0.2	3.818	0.250 / 0.800	0.192

Table 1. Assumed Mechanical Characteristics of the Stone Masonry

Next, certain commonly used masonry failure criteria were adopted for either in-plane tension-compression or out-of-plane tension. All the masonry parts of the studied structures were examined in terms of in-plane and out-of-plane stress demands posed by the considered load combinations against the corresponding capacities, as these capacities were obtained by applying the Mohr-Coulomb criterion of equation 1 or the stone masonry compressive and tensile strength limits listed in Table 1. Due to space limitations such results are not shown in detail here. Selective results obtained from this evaluation process are shown in figures 10, 12 and 14. With R_σ or with R_τ the ratio of the in-plane tensile or shear strength value over the corresponding demand is signified, whereas with R_M the ratio of the out-of-plane tensile strength value over the corresponding demand is denoted. Ratio values smaller than one ($R_\tau, R_\sigma, R_M < 1$) predict a corresponding limit state condition. As can be seen, the followed methodology is based on combining numerical stress demands resulting from elastic analyses with limit-state strength values. A different approach is to combine these limit-state strength values with a non-linear push-over type of analyses, as was done by Manos et al. [2]. It was shown that the methodology applied here correlates quite well with the non-linear approach proposed by Manos et al. [2], in predicting regions of structural damage.

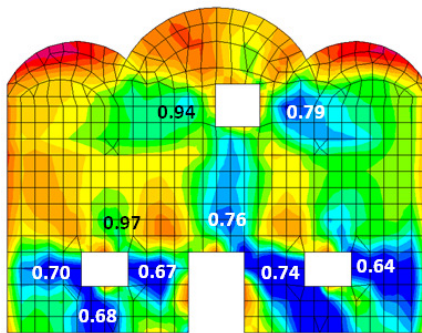


Figure 10a. Internal Transverse Wall, 0.9G+1.4Ey , Non-Deformable Foundation, Max in-plane shear stress strength / demand ratio R_τ

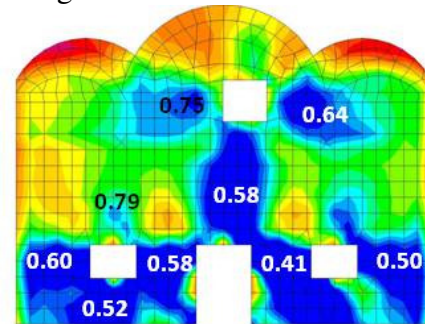
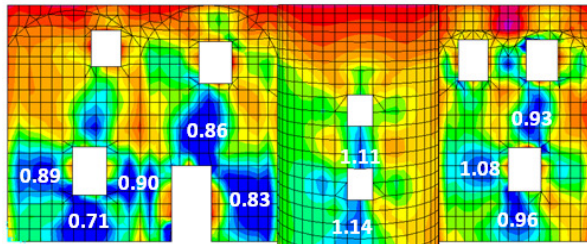
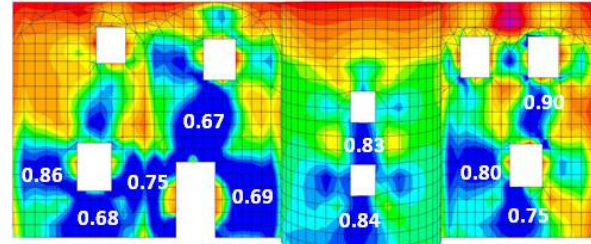


Figure 10b. Internal Transverse Wall, 0.9G+1.4Ey , Deformable Foundation, Max in-plane shear stress strength / demand ratio R_τ

Figures 10a and 10b depict the R_τ ratio values of the in-plane shear strength / shear demand for the load combination 0.9G+1.4Ey. The structural element that these ratio values belonged to is the internal transverse wall which separates the main church from the women's quarters situated at the west portion of the church (see figures 5a). This wall as well as internal faces of all the peripheral walls, vaults and domes are decorated with very valuable frescos that bear signs of extensive damage (see figures 9 and 11).



Figure 11. Damage of the Internal Transverse Wall and the adjacent arch

Figure 12a. Non-Deformable Foundation South Peripheral Longitudinal Wall, 0.9G+1.4Ex, Ratio values of R_{τ} in-plane shear strength / shear demandFigure 12b. Deformable Foundation South Peripheral Longitudinal Wall, 0.9G+1.4Ex, Ratio values of R_{τ} in-plane shear strength / shear demand

This damage is also predicted by the numerical analysis results as can be seen from the strength / demand R_{τ} ratio values that are well below one ($R_{\tau} < 1$) in many locations (Figures 12a and 12b). Moreover, the deformability of the foundation leads this ratio to obtain even smaller values than for the case of the non-deformable foundation, which demonstrates the detrimental effect of the flexibility of the foundation for this church. The deformability of the foundation has such an effect in almost all peripheral walls; this can be established by either comparing the values of the in-plane shear strength / demand ratio R_{τ} (figures 12a and 12b) or the out-of-plane tensile strength / demand ratio R_M (see figures 13a and 13b), that is also visible at the outer face (figures 14).

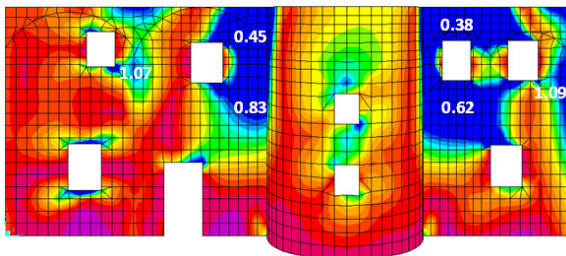
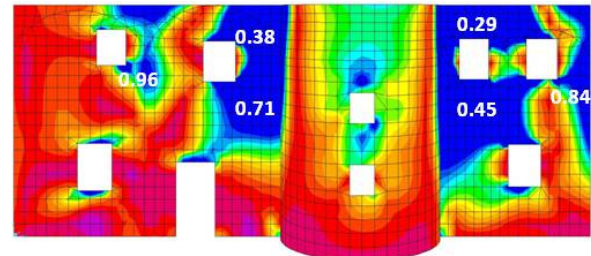
Figure 13a. Non-Deformable Foundation South Peripheral Wall, 0.9G+1.4Ey, Ratio values of R_M out-of-plane σ_{11} normal strength / demand (Top face)Figure 13b. Deformable Foundation South Peripheral Wall, 0.9G+1.4Ey, Ratio values of R_M out-of-plane σ_{11} normal strength / demand (Top face)

Figure 14. Damage of the peripheral masonry walls.

4 THE CHURCH OF PROFITIS ILIAS AT SIATISTA - KOZANI

This is also a Post-Byzantine three nave Basilica built in 1701 A.D. on the top of a hill in the town of Siatista of the prefecture of Kozani. It also has a wooden roof without the vaulting system of the Post-Byzantine Basilica described in section 2.

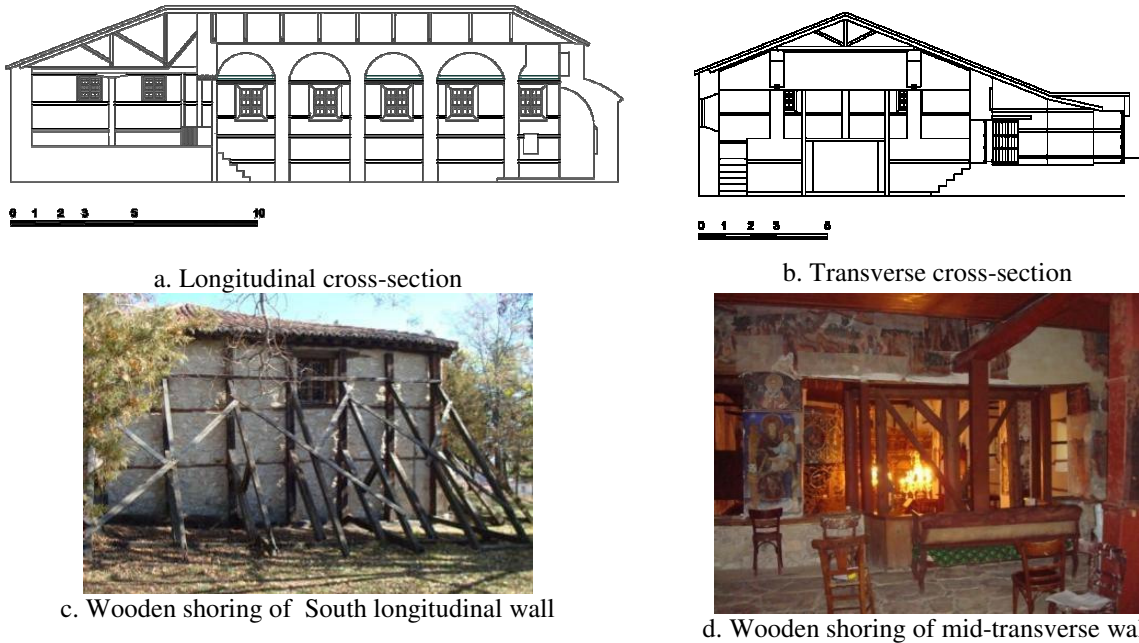


Figure 15. The church of Profitis Ilias at Siatista - Kozani

The horizontal dimensions of this church are 23.25m in length and 16.60m in width. The top of the roof lies at 7.1m from the floor level of the interior of this church. The naves are formed by 4-column colonnades (figures 15a and 15b) built with stone masonry. The lower part of the key of each arch of these colonnades lies at 5.25m from the floor level of the interior of this church. All the exterior walls are made of stone masonry. Apart from the main church a narthex was built at the North side at a later stage; this narthex is of a lower height than the main church. The West part of the church is allocated to the women quarters that is separated from the rest of the interior by a mid- transverse wall (figure 15d). The South longitudinal wall is supported by a system of wooden beams as is shown in figure 15c. These were installed after the Kozani-1995 earthquake sequence. Additional wooden supports are also placed at the mid-transverse wall (figure 15d) as well as at the mid-span of a longitudinal beam that spans the women quarters from East-West. According to past records, the structural system of this church showed signs of distress from soil-settlement sometime before the occurrence of this particular earthquake sequence. The records do not give information of any countermeasures being taken in the past up to the point of the earthquake occurrence. The main structural damage, as recorded after this earthquake sequence, is described below. Inclination of the South longitudinal wall outwards that is accompanied with extensive cracking at its joints with the East and West exterior masonry walls as well as with the mid-transverse wall. Extensive cracking is also evident at the East wall with the apses (figure 16a) and at the arches of the colonnades (figure 16b). Despite the fact that 18 years have passed since this earthquake damage, the counter measures so far are in the form of the temporary wooden shoring as well as the renovation of the wooden roof.



Figure 16a. Extensive cracking of the apse at the East wall



Figure 16b. Extensive cracking at the joint of the South longitudinal wall with the mid-transverse wall with its wooden shoring

4.1. Numerical Simulation including the influence of the soil deformability

The current numerical investigation of this church included the following:

- Simulation of the behavior assuming non-deformable supports at the foundation level.
- Simulation of the behavior assuming deformable supports at the foundation level, introducing at this level elastic springs with properties reflecting the actual soil deformability that was found from in-situ sampling.

The soil consists of clay in its upper layers. For quantifying the stiffness of these soil layers use was made of the data from three boreholes drilled in the vicinity of the church relevant to the constitution of the soil deposits at a depth up to 15m (see figure 17)

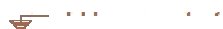
					
$\gamma = 21 \text{ KN/m}^3$	$N > 60$	$c = 2 \text{ KPa}$	$\varphi = 30^\circ$	$E_s = 20 \text{ MPa}$	
2.00- 2.70m					
$\gamma = 20 \text{ KN/m}^3$	$N > 60$	$c_u = 160 \text{ KPa}$	$c' = 30 \text{ KPa}$	$\varphi' = 22^\circ$	$E_s = 17 \text{ MPa}$
4.70- 6.00m					
$\gamma = 25 \text{ KN/m}^3$	$c = 200 \text{ KPa}$	$\varphi = 30^\circ$	$E_s = 5000 \text{ MPa}$		
5.00- 15.20m					

Figure 17. Properties of the Soil Profile obtained from boreholes drilled in the vicinity of the church

All the numerical simulations assumed elastic behaviour with relatively low-values of the modulus of elasticity for the stone masonry equal to $E=1660\text{MPa}$. The thickness of the masonry walls varied from 0.75m to 1.0m. The system of the wooden roof was modeled as well as all the wooden elements that connect the longitudinal and transverse walls with the interior colonnades and the mid-transverse wall. Figure 18 depicts the numerical predictions of the displacement response of this church when it is subjected to only gravitational loads

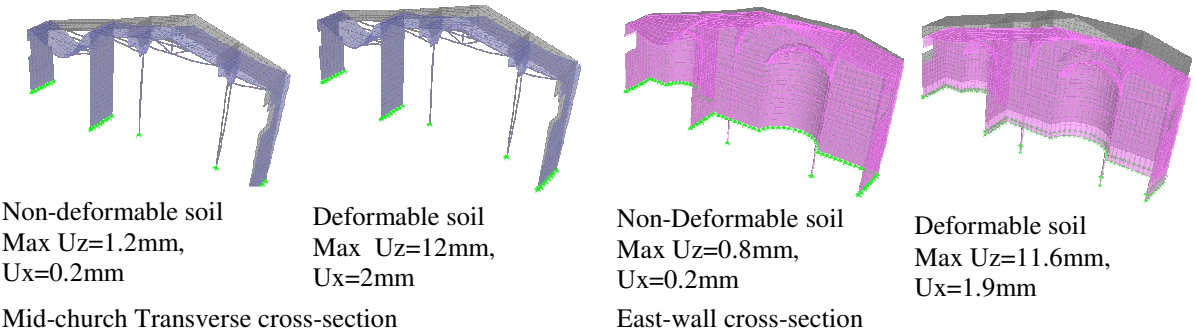


Figure 18. Deformations for gravitational forces (Non-deformable / Deformable foundation)

A small number of mortar specimens were taken from this church. Some basic properties of these mortar samples are listed in Table 2. Moreover, the type of natural stone used in the masonry elements is a type of slate with a compressive strength equal to 24MPa, as given in the literature survey.

Mortar Sample code name	Absorption %	Specific gravity KN/m ³	Porous count %
K1	5.312	22.51	11.95
K2	0.51	27.22	13.89

Table 2. Characteristics of mortar samples taken from the church

Table 3 lists the assumed mechanical characteristics for the stone masonry in terms of Young's modulus and Poisson's ratio as well as compressive and tensile strength values. These values were based mainly from data included in the literature. From the comparison of the limit strength values of Table 3 with those of Table 1 it can be easily seen that the stone masonry of the church of Profitis Ilias of Siatista is much weaker than that of the church of Agia Triada at Vithos.

	Young's Modulus (N/mm ²)	Poisson's Ratio	Compressive Strength (N/mm ²)	Tensile Strength normal / parallel bed-joint (N/mm ²)	shear strength f_{vko} (N/mm ²)
Limit values	1660	0.2	1.0	0.10 / 0.25	0.10

Table 3. Assumed Mechanical Characteristics of the Stone Masonry

Moreover, a Mohr-Coulomb failure envelope was adopted for the in-plane shear limit state of the stone masonry, when a σ_n normal stress is acting simultaneously, that is defined through the following relationship that is the same as equation (1) described before in section 3 ([2], [3], [4], [5], [6], [7], [8], [11]).

$$f_{vk} = f_{vko} + 0.4 \sigma_n \quad (1)$$

As was done before the values of the strength over demand ratios at the most critical locations of the masonry walls and vaults were obtained by comparing the strength values listed in table 3 with the corresponding demand values as they were obtained from the numerical simulation. The ratio of the in-plane tensile or shear strength value over the corresponding demand is signified by \mathbf{R}_σ or \mathbf{R}_τ whereas with \mathbf{R}_M denotes the ratio of the out-of-plane tensile strength value over the corresponding demand. Ratio values smaller than one ($\mathbf{R}_\tau, \mathbf{R}_\sigma, \mathbf{R}_M < 1$) predict a corresponding limit state condition

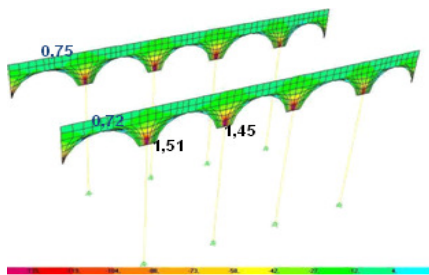


Figure 19a. G+0.3Q. Non-Deformable soil \mathbf{R}_σ Ratio of in-plane strength / demand $\mathbf{F22}$ (KN/m) normal to bed joint

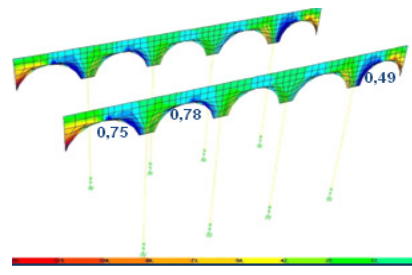


Figure 19b. G+0.3Q. Deformable soil Ratio \mathbf{R}_σ of in-plane strength / demand $\mathbf{F22}$ (KN/m) normal to bed joint

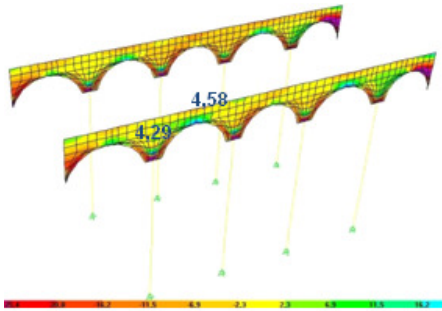


Figure 19c. G+0.3Q. Non-Deformable soil R_{σ} Ratio of in-plane strength / demand F_{11} (KN/m) parallel to bed joint

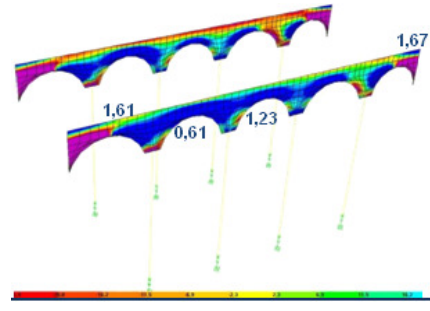


Figure 19d. G+0.3Q. Deformable soil R_{σ} Ratio of in-plane strength / demand F_{11} (KN/m) parallel to bed joint

These R_{σ} ratio values of in-plane strength / demand applying the limit tensile strength scenario, either normal to bed-joint (F_{22}) or parallel to bed-joint (F_{11}) are depicted in figures 19a to 19d for the masonry arches above the internal colonnades. The demands in these figures were obtained for the load combination G+0.3Q. As can be seen from these figures the R_{σ} ratio values are smaller for the deformable than the non-deformable foundation, which demonstrates the detrimental effect of the foundation deformability for this church even only for the gravitational forces.

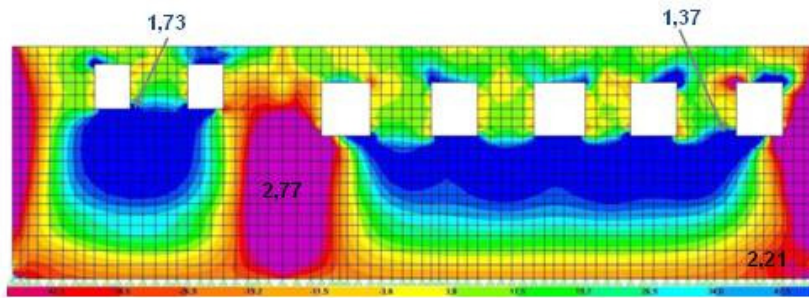


Figure 20a. Non-Deformable soil 0.9G+1.4E_y. R_M Ratio out-of-plane strength / demand σ_{11} (KN/m²) Outer-face.

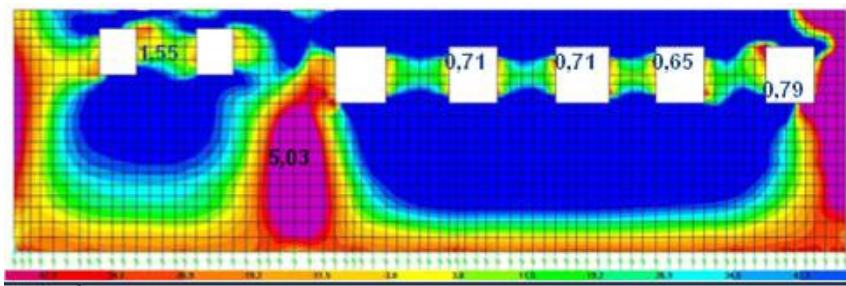


Figure 20b. Deformable soil 0.9G+1.4E_y. R_M Ratio out-of-plane strength / demand σ_{11} (KN/m²) Outer-face.

For the load combination 1.3G+1.5Q, that dictates the design for the gravitational forces under current code provisions, the above ratio values will become even smaller, which signifies that the colonnades cannot withstand the maximum gravitational forces. This is verified by the observed damage which is quite evident for these structural elements in this church as it stands today being supported after the earthquake event of 1995 by temporary wooden shoring internally as well as externally (see figure 15c, 15d, 16a and 16b). The numerical simulation was also repeated for the load combinations either 0.9G+1.4E_x or 0.9G+1.4E_y. Initially this was done with the seismic loads considered as static forces either E_x or E_y generated at the existing masses by a constant acceleration of such value that results in the same base shear value that was found when the earthquake actions were considered through a dy-

dynamic spectral analysis as will be explained below. In figures 20a and 20b the R_M ratio out-of-plane strength / demand (σ_{11}) (KN/m^2) are depicted. The numerical simulation was repeated to include the seismic actions in the form of dynamic spectral analysis utilising the design spectrum derived by applying the provisions of the current Greek Seismic code for seismic zone I, soil category B and importance factor 1.3 [10] .

Non-Deformable Foundation

Deformable Foundation

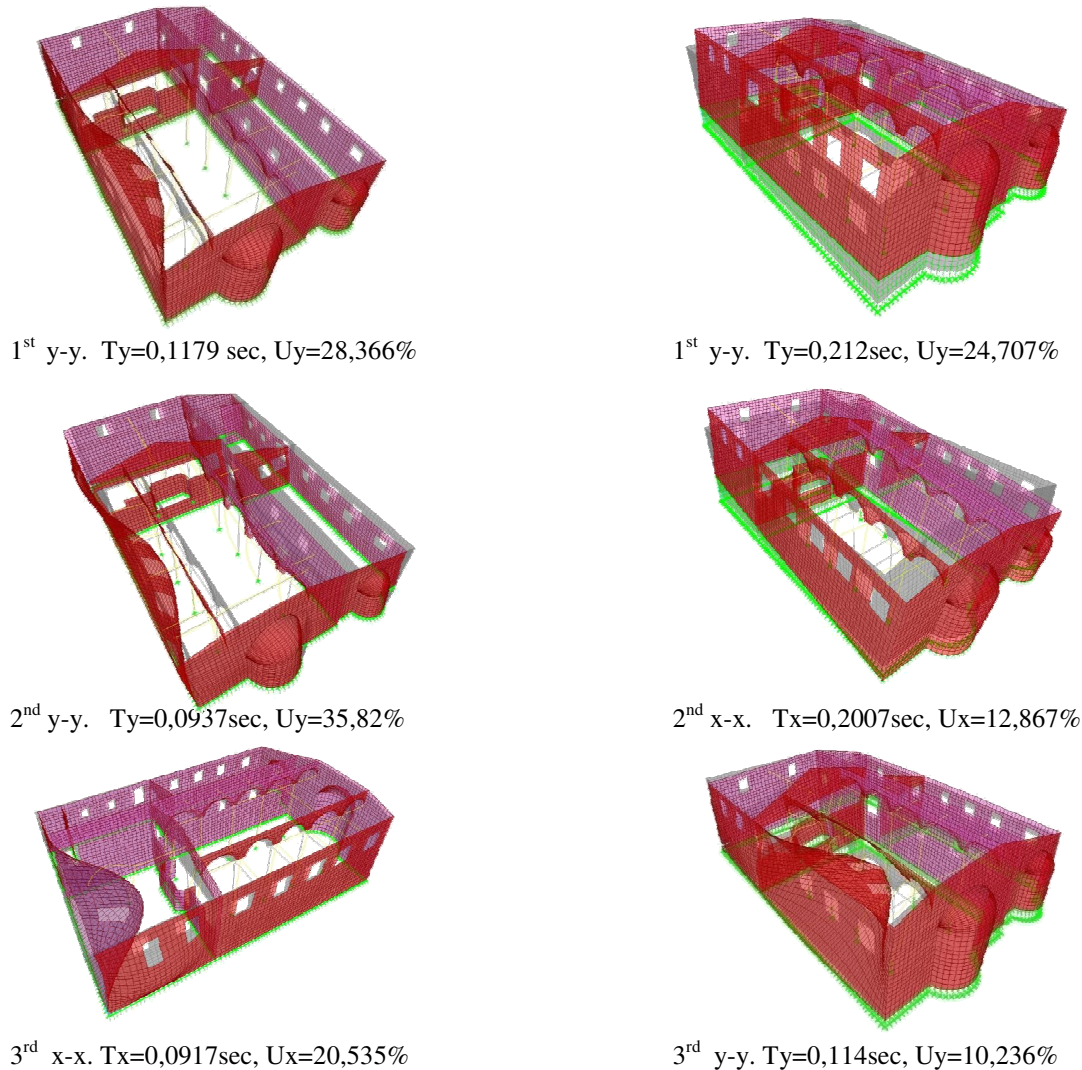


Figure 21. The most significant eigen-modes for the non-deformable and the deformable foundation together with the values of the corresponding eigen-frequencies and modal mass participation ratios.

This dynamic spectral analysis was based on a sufficient number of eigen-modes capable of mobilising sums of modal mass larger than 65% of the total mass of the structure. Figures 21 depict the most significant translational x-x and y-y eigen-modes together with their corresponding eigen-period and modal mass ratio values. This is done for both the non-deformable as well as the deformable foundation numerical models. As was also observed previously, the modal analysis results demonstrate the first effect of the deformable foundation which is the lengthening of the eigen-periods of the most significant translational modes.

From the evaluation of the demands obtained from the numerical simulation as compared with the limit strength values adopted for the stone masonry of this church it can be concluded that the deformability of the foundation results in strength / demand ratio values (R_r , R_σ , R_M) smaller than the corresponding ratio values for the non-deformable foundation.

These results signify the existence of critical regions for the various masonry structural elements that cannot withstand the demands, as they were quantified by the numerical analyses and the current code provisions. Such an evaluation can explain, up to a point, the development of the existing current state of structural damage. Gaining such confidence in the employed methodology, the designer also gains the advantage in evaluating with the same methodology the effectiveness of a potential retrofitting scheme. In order for such a retrofitting scheme to be effective, the resulting strength / demand ratios should attain values larger than the corresponding values without this retrofitting scheme and, if possible, larger than one ($R_\tau, R_\sigma, R_M > 1$).



Figure 22. South Peripheral Wall. Regions with small values of the strength / demand R_M out-of-plane tensile behaviour (orange), R_σ in-plane tensile behaviour (blue)

Such an evaluation has been performed for the most vulnerable structural elements of this church; that is the internal colonnades, the South and North peripheral walls and the East peripheral wall with the apses. The predictions by the numerical analysis of potential damage regions is indicated with the strength / demand ratio values well below one ($R_\tau, R_\sigma, R_M < 1$). These predictions are depicted in figure 22 through the values of ratio R_σ (in-plane tensile behaviour, blue), ratio R_M (out-of-plane tensile behaviour, orange). In almost all structural elements the out-of-plane tensile behaviour results in strength / demand ratios with values well below one ($R_M < 1$). The smallest R_M ratio value appears at the South longitudinal peripheral wall and is approximately equal to $R_M = 0.15$. The average value of this R_M ratio obtained by averaging the corresponding values at six (6) different locations well spread over the entire length of this wall is equal to 0.245. This strongly indicates that the existing capacity of this wall in out-of-plane bending is exceeded fourfold by the corresponding demands. It is not surprising that this wall has visible signs of out-of-plane displacements that are in agreement with such a state of distress, as predicted by the followed methodology.

5 RETROFITTING - EXPERIMENTAL INVESTIGATION.

Retrofitting of heritage structures is, in general, a difficult task as it cannot employ traditional retrofitting techniques that have been developed for reinforced concrete structures ([12], [13], [14]). The latter can be termed as strong non-reversible interventions, because such retrofitting schemes usually do not respect the principles either of compatibility of the old materials with the new materials or that of reversibility of the employed intervention scheme. The latter is thought to be a necessary feature of a retrofitting scheme, intended to be applied on a heritage structure, so that it can be potentially replaced by a more efficient retrofitting scheme in the future. Such a retrofitting scheme for heritage structures can mobilize the following:

- The upgrading of the strengths of the existing masonry. This is usually achieved, up to a point, with compatible mortars that can be injected with low pressure and fill the voids of the existing weak stone masonry (see section 5.1.).

- The strengthening of the wooden parts of the roof and their connection to the masonry.
- The replacement of the wooden elements or ties and the addition of new metal ties.
- The strengthening of the foundation with various forms of external or internal encasement schemes. This was studied for the church of the Virgin Mary at Dilofo (section 2, [9]).
- Semi-temporary external shoring employing wooden, metal or reinforced concrete parts.
- The utilization of more advanced retrofitting methods, such as base isolation in an effort to lower the demands. This, although desirable, can encounter significant construction difficulties ([15], [16], [17], [18]).

Temporary wooden shoring, internal as well as external, was proposed and partly employed in the cases of the church of the Virgin Mary at Dilofo and Profitis Ilias at Siatista (see figures 15c and 16a). Such temporary wooden shoring, although erected until it is replaced by the permanent retrofitting scheme, usually remains in many applications for considerably long periods. However, the connections of such a temporary scheme to the structure and the surrounding soil become less effective with time under a variety of environmental influences that they were not designed for, rendering such a scheme ineffective

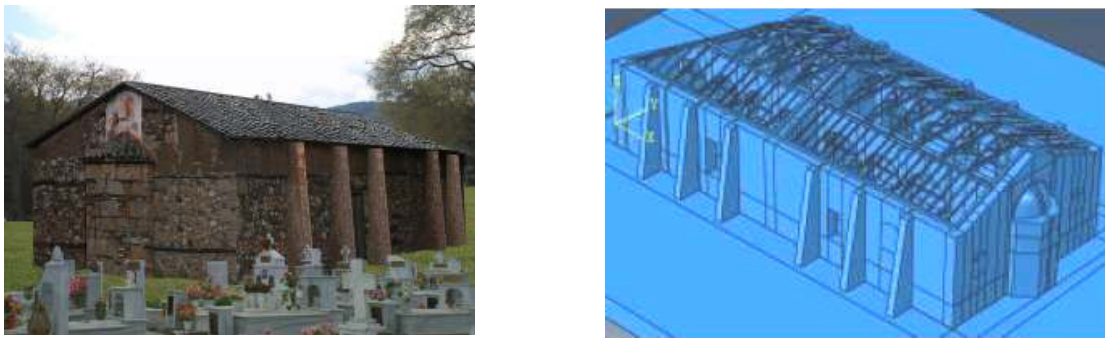


Figure 23. The church of Agios Dimitrios at Palatitsia

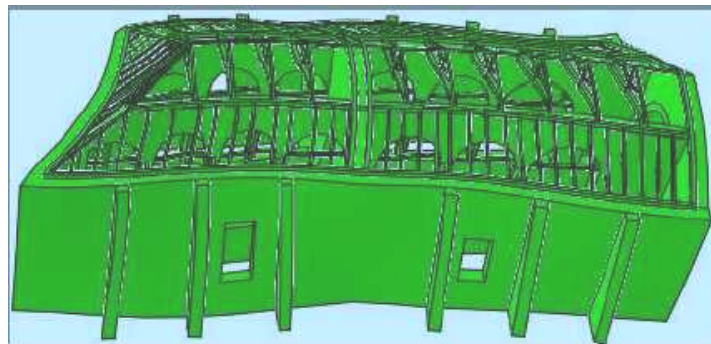


Figure 24a. 2nd x-x Translational eigen-mode. $T_x=0,2013\text{sec}$, $U_x=38,5\%$

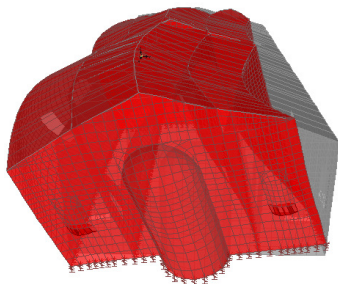


Figure 24b. Present condition, deformable foundation, Main Transversal y-y eigen-mode, $T_y = 0,326\text{sec}$ $U_y=61,62\%$

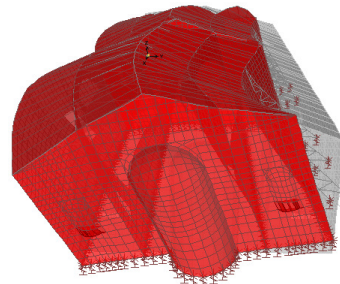


Figure 24c. Retrofitted with seimi-permanent shoring. Deformable foundation, Main Transversal y-y eigen-mode, $T_y = 0,263\text{sec}$ $U_y=68.17\%$

Semi-permanent shoring must be designed and constructed respecting the principle of reversibility. Moreover, it can be combined with the rest of the reversible techniques mentioned above, taking into consideration environmental influences. Such a retrofitting scheme is currently being investigated to be applied at Agios Dimitrios at Palatitsia Imathias, a 16th century three-nave Basilica. This church is 27.10m long on its South side and 22.15m long on its North side with an average width 12.625m. The height from the ground level to the top of the roof is 6.75m (figure 23). The studied retrofitting scheme consists of a system of semi-temporary external shoring of the longitudinal peripheral walls together with the upgrading of the wooden roof, the replacement of the internal wooden ties and the addition of new metal ties as well as mortar injections for all stone masonry. The performance of such a retrofitting scheme was investigated numerically by a full dynamic analysis (figures 24) employing the methodology described in sections 2, 3 and 4.

This retrofitting scheme in the current investigation takes a variety of alternative forms. The numerical results so far provide sufficient evidence that such a retrofitting scheme can be quite effective in upgrading the performance of the various stone masonry elements in such a way that the strength / demands ratio values R_r in-plane shear, R_σ in-plane tension, and R_M out-of-plane tensile flexure, described in sections 2, 3 and 4 before, obtain values larger than the corresponding values for the current state of stress before any intervention. The objective of the current study is for these strength / demands ratio values to reach the threshold value of 1, ideally at all critical locations, thus signifying acceptable performance. Typical results are shown in figures 25 for the out-of-plane σ_{22} demands. This is done for both the existing condition (figure 25a) as well as for the condition after the previously described retrofitting scheme is applied (figure 25b). The existing state of stress includes large areas in the vicinity of the window openings with considerable tensile stress concentration exceeding the strength values, thus indicating potential structural damage regions. The introduction of the proposed retrofitting resulted in a considerable decrease of these out-of-plane σ_{22} demands. This decrease in the demands when combined with an increase in the strength values, achieved from injecting the stone masonry with compatible mortar, results in values of the strength / demands ratios (R_r in-plane shear, R_σ in-plane tension, and R_M out-of-plane tensile flexure) nearing the threshold value of one, thus satisfying the objective of the retrofitting scheme.

Present condition

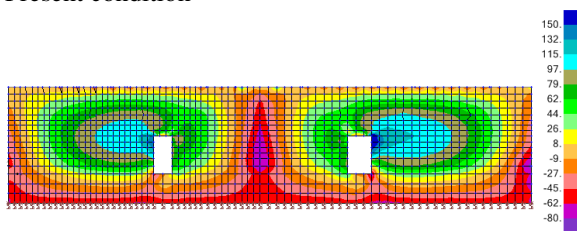


Figure 25a. South Longitudinal Wall, G+0.30Q+Ey Present condition, deformable foundation, σ_{22} (kN/m², Kpa)- normal stress - Bottom face.

Retrofitted with semi-temporay metal shoring

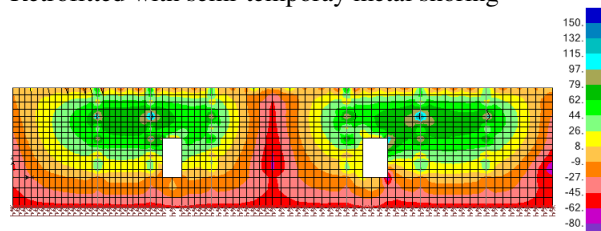


Figure 25b. South Longitudinal Wall, G+0.30Q+Ey Retrofitted with semi-temporay metal shoring, deformable foundation, σ_{22} (kN/m², Kpa)- normal stress - Bottom face.

5.1. Shear capacity of stone masonry - summary of experimental testing

A number of stone masonry specimens were built at the laboratory using lime mortar and natural stones. The lime mortar had such a composition as to be representative of old relatively weak mortars commonly used in the past. A series of such samples were tested accompanied by constant compression with variable shear as shown in figure 26b. This set-up was designed in an effort to record the shear force at a limit state which represented the failure of the mortar bed-joint as depicted in figures 26c,d. Based on these experimental results, the

the mortar bed-joint as depicted in figures 26c,d. Based on these experimental results, the Mohr-Coulomb limit state criterion (figure 26a, equation 1) can be approximately quantified.

Mohr Coulomb failure criterion $f_v = f_{vo} + 0.45 \sigma$
 $f_{vo} = 0.12 \text{ Mpa}$

	Normal Stress σ (Mpa)	Predicted $f_v =$ $f_{vo} + 0.45 \sigma$ (Mpa)	Measured value f_v (Mpa)	Ratio Measured f_v / Predicted f_v
Sample 1	0.53	0.359	0.396	1.103
Sample 2	0.61	0.395	0.41	1.038
Sample 3	0.46	0.327	0.305	0.933
Sample 4 α	0.30	0.255	0.20	0.784
Sample 4 β	0.54	0.363	0.375	1.033

Figure 26a. Verification of the Mohr-Coulomb criterion



Figure 26b. Experimental set-up



Figure 26c. Sliding mode of failure



Figure 26d. Sliding mode of failure

Following these initial samples, another sequence of tests will be performed aimed at quantifying the Mohr-Coulomb failure envelope representing old stone masonry that was injected in the framework of a mild retrofitting scheme. The injected mortar should be of such a composition as: a) to be compatible with the existing materials b) to be able to fill the existing voids and c) to result in higher strength values. This experimental sequence is still under way.

6 CONCLUSIONS

1. The eigen-periods, eigen-modes, and the deformation patterns to horizontal earthquake actions of the examined churches, predicted numerically, document that the longitudinal peripheral walls develop much larger out-of-plane displacements at their top than in-plane displacements. Moreover, the presence of the apses exercise a significant out-of-plane stiffening effect. The presence of stone masonry vaulting system increases the stiffening effect at the top of the peripheral wall level; however, such a vaulting system also adds considerable masses at a high level which generate seismic actions of large amplitude.

2. The numerical stress results together with assumed strength values for the various masonry elements of the examined churches predict that the regions most vulnerable to damaged are near the door and window openings for the in-plane behavior. These regions together with the regions near the foundation appear to be the most vulnerable to out-of-plane bending, particularly for the longitudinal masonry walls. Such numerical predictions of structural damage are in reasonably good agreement, in a qualitative sense, with actual observed damage. This is despite the fact that the numerical simulation is based on elastic analysis assumptions. The employed limit state criteria of strength / demands ratio values (R_r in-plane shear, R_o in-plane

tensile, and \mathbf{R}_M out-of-plane tensile behaviour) lead to successful predictions of actual distress of the peripheral walls. When the superstructure consists of vaults and domes large seismic forces are generated that lead to areas of stress concentration at the bases of the domes and vaults and at the keys of the arches. Further investigation is needed to establish appropriate limit-state criteria for these stone masonry elements.

3. The foundation deformability was also investigated by introducing linear deformable springs at the foundation level. The results of such a numerical approximation combined with the followed methodology of limit state criteria of strength / demands ratio values (\mathbf{R}_τ in-plane shear, \mathbf{R}_σ in-plane tensile, and \mathbf{R}_M out-of-plane tensile behaviour) demonstrated in all the examined cases that the foundation deformability, when combined with the gravitational forces and seismic actions, leads to \mathbf{R}_τ , \mathbf{R}_σ , and \mathbf{R}_M strength / demands ratio values that are considerably smaller than for the case of non-deformable foundation, thus verifying the detrimental effect of the foundation deformability in all the examined cases.

4. A retrofitting scheme, which combines mortar grouting, wooden and metal ties, external semi-temporary shoring of the longitudinal walls together with foundation encasement is being currently investigated. The numerical results so far provide sufficient evidence that such a retrofitting scheme can be quite effective in upgrading the performance of the various stone masonry elements in such a way that the \mathbf{R}_τ , \mathbf{R}_σ , and \mathbf{R}_M strength / demands ratio values are larger than the corresponding values for its current state before any intervention. The objective of the current study is for these strength / demands ratio values to reach the threshold value of 1, ideally at all critical locations, thus signifying acceptable performance.

5. An experimental sequence is also in progress that tries to quantify combined shear and compression limit-state criteria for stone masonry specimens that represent parts of the stone masonry walls prior to any intervention with compatible mortar injections.

REFERENCES

- [1] Manos George, "Consequences on the urban environment in Greece related to the recent intense earthquake activity", *Int. Journal of Civil Engineering and Architecture*, Dec. 2011, Volume 5, No. 12 (Serial No. 49), pp. 1065–1090.
- [2] Manos G.C., Soulis V., Diagouma A. (2008) "Numerical Investigation of the behavior of the church of Agia Triada, Drakotrypa, Greece", *Journal in Advances in Engineering Software* 39 (2008) 284-300.
- [3] G.C. Manos, V.J. Soulis, O. Felekidou, "The dynamic and Earthquake Behavior of Greek Post-Byzantine Churches", 14WCEE, Beijing, CHINA, 2008.
- [4] G. C. Manos, V. J. Soulis, O. Felekidou, A. Koutsianou, P. Lipiridou, «The dynamic and earthquake response of Greek Byzantine and Post-Byzantine Basilicas», COMDYN 2009, Rhodes, Greece.
- [5] G.C Manos, V. Soulis, N. Karamitsios, O. Felekidou, Numerical Simulation of the Dynamic and Earthquake Behaviour of Greek Post-Byzantine Churches with and without Base Isolation", PROHITECH 2009, 21 to 24 June 2009, Rome, Italy.

- [6] Manos George, Soulis V., Felekidou O., “Numerical Study of the Dynamic and Earthquake Behavior of Byzantine and Post-Byzantine Basilicas”, 8th International Masonry Conference, 2010, Dresden, Germany.
- [7] Manos George, Soulis V., Felekidou O., Matsou V. “A Numerical Investigation of the Dynamic and Earthquake Behavior of Byzantine and Post-Byzantine Basilicas”, 9th U.S. National and 10th Canadian Earthquake Engineering Conference, 2010, Canada.
- [8] Manos George, Soulis V., Felekidou O., Matsou V. “A Numerical Investigation of the Dynamic and Earthquake Behavior of Byzantine and Post-Byzantine Basilicas”, 3rd International Workshop on Conservation of Heritage Structures Using FRM and SHM, 2010, Ottawa, Canada.
- [9] G.C. Manos “The bearing capacity of the Assumption of Virgin Mary, a three-nave Basilica at Dilofo-Voio-Kozani and a retrofitting proposal”, Technical Report to the Greek Ministry of Culture, April, 2011 (in Greek).
- [10] Provisions of Greek Seismic Code 2000, Organization of Earthquake Planning and Protection of Greece OASP, Dec. 1999 published by OASP. Revisions of seismic zonation introduced in 2003, Government Gazette, Δ17α /115/9/ΦΝ275, No. 1154, Athens, 12 Aug. 2003.
- [11] European Committee for Standardization, Euro code 6; “Design of Masonry Structures, Part 1-1:General Rules for Building. Rules for Reinforced and Un-reinforced Masonry”, EN 1996-1-1:2005.
- [12] Earthquake Engineering Retrofitting of Heritage Structures “Design and evaluation of strengthening techniques”, Edited By: S. Syngellakis, Wessex Institute of Technology, UK, ISBN: 978-1-84564-754-4, eISBN: 978-1-84564-755-1, Published: 2013.
- [13] G. C. Manos and E. Papanou, “Earthquake Behaviour of a R/C Building Constructed in 1933 before and after its Repair” STREMAH 2009, Tallin, 22-24 June, 2009.
- [14] Organization of Earthquake Planning and Protection of Greece (OASP), Guidelines for Retrofitting in Reinforced Concrete Buildings, Government Gazette, Δ17α /04/5/ΦΝ 429-1, No 42, Athens, 20 Jan. 2012.
- [15] G. C. Manos, V. Soulis, O. Felekidou, N. Karamitsios, L. Kotoulas, “Numerical Study of the Dynamic and Earthquake Response of Greek Post-Byzantine Churches with or without Base Isolation”, 3rd International Workshop on Conservation of Heritage Structures Using FRM and SHM, 2010, Ottawa, Canada.
- [16] G.C. Manos, N. Karamitsios, “ Numerical Simulation of the Dynamic and Earthquake Behavior of Greek Post-Byzantine Churches with and without Base Isolation”, COMPDYN 2011, Corfu, Greece, 26–28 May 2011.
- [17] G.C. Manos, N. Karamitsios, “Study of the Dynamic and Earthquake Response of Greek Post-Byzantine Churches with and without Base Isolation” EURO DYN 2011, Leuven, Belgium, 4-6 July, 2011.
- [18] G. C. Manos and N. Karamitsios, “Earthquake Numerical Simulation of the Dynamic and Earthquake Behaviour of Greek Post-Byzantine Churches with and without Base Isolation”, STREMAH-2011, Chianciano, Italy, Sep. 2011.
- [19] V. Dimitriadis “An ordinance for the erection of the first church in Gianitsa”, Meke-donika, Vol. 9, Society for Mecedonian Studies, Thessaloniki 1969.